Pharm Res (2018) 35: 24
https://doi.org/10.1007/s11095-017-2320-2

RESEARCH PAPER

Decorated Superparamagnetic Iron Oxide Nanoparticles with Monoclonal Antibody and Diethylene-Triamine-Pentaacetic Acid Labeled with Thechnetium-99m and Galium-68 for Breast Cancer Imaging

Marta de Souza Albernaz[1,2,3] • Sergio Hiroshi Toma[3] • Jeff Clanton[2,4] • Koiti Araki[3] • Ralph Santos-Oliveira[2,5]

Received: 28 October 2017 / Accepted: 21 November 2017 / Published online: 5 January 2018

ABSTRACT

Purpose In this study we developed and tested an iron oxide nanoparticle conjugated with DTPA and Trastuzumab, which can efficiently be radiolabeled with 99m-Tc and Ga-68, generating a nanoradiopharmaceutical agent to be used for SPECT and PET imaging.

Methods The production of iron oxide nanoparticle conjugated with DTPA and Trastuzumab was made using phosphorylethanolamine (PEA) surface modification. Both radiolabeling process was made by the direct radiolabeling of the nanoparticles. The *in vivo* assay was done in female Balb/c nude mice xenografted with breast cancer. Also a planar imaging using the radiolabeled nanoparticle was performed.

Results No thrombus and immune response leading to unwanted interaction and incorporation of nanoparticles by endothelium and organs, except filtration by the kidneys, was observed. In fact, more than 80% of ^{99m}Tc-DTPA-TZMB@Fe_3O_4 nanoparticles seems to be cleared by the renal pathway but the implanted tumor whose seems to increase the expression of HER2 receptors enhancing the uptake by all other organs.

Conclusion However, even in this unfavorable situation the tumor bioconcentrated much larger amounts of the nanoagent than normal tissues giving clear enough contrast for breast cancer imaging for diagnostics purpose by both SPECT and PET technique.

KEY WORDS imaging · nanoradiopharmaceuticals · oncology · smart device

ABBREVIATIONS

@Fe_3O_4	Iron oxide nanoparticles
99mTc	Technetium 99 metastable
BT-474	Invasive ductal carcinoma cell line
DTPA	Diethylene triamine pentaacetic acid
GA	Glutaraldehyde
Ga-68	Gallium-68
Ge^{68}– Ga^{68}	Germanium 68 – Gallium-68
GIST	Gastrointestinal stromal tumor
HER2 receptors	Human epidermal growth factor receptor 2
ITLC-SG	Instant Thin Layer Chromatography – Silica Gel
IV	Intravenous
MBq	Mega Becquerel
mCi	Mili Curie
PEA	Phosphorylethanolamine
PET	Positron Emission Tomography
ROI	Regions of interest
RPMI	Roswell Park Memorial Institute médium
SC	Subcutaneous
SPECT	Single Photon Emission Computed Tomography
SPIONs	Superparamagnetic iron oxide nanoparticles
TEM	Transmission Electron Microscopy
TZMB	Trastuzumab

✉ Koiti Araki
koiaraki@iq.usp.br

✉ Ralph Santos-Oliveira
roliveira@ien.gov.br

1 Radiopharmacy Service, University Hospital Clementino Fraga Filho, Rio de Janeiro, Brazil

2 Instituto de Pesquisas Energéticas e Nucleares, Centro de Radiofarmácia, São Paulo, Brazil

3 Department of Fundamental Chemistry, Institute of Chemistry, University of São Paulo, Av. Prof. Lineu Prestes 748, São Paulo, SP 05508-000, Brazil

4 Department of Radiology, Vanderbilt University Medical Center, Nashville, Tennessee, USA

5 Brazilian Nuclear Energy Commission, Nuclear Engineering Institute, Rio de Janeiro, Brazil

INTRODUCTION

Among all malignant tumors breast cancer is the most prevalent type in women, as confirmed by the more than 1.7 million new diagnosed cases per year, representing about 25% of total female patients with cancer worldwide (16).

Several strategies have been implemented in recent decades, consisting of early diagnosis actions and tracking (7,9). However, in countries with medium and low income, breast cancer is diagnosed only at advanced stages, compromising the treatment and the quality of life of patients (40). Thus, the implementation of a whole set of advanced diagnostic methods designed for early detection of breast cancer is of fundamental relevance to change the current scenario.

Among the new strategies addressing diagnosis and treatment of cancer, the use of formulations based on monoclonal antibodies is the most successful ones (17). In this direction, the first clinically approved monoclonal antibody for treatment of metastatic breast cancer was Trastuzumab (Herceptin®), whose mechanism of targeting is dependent on the increased number of HER2 receptors (19,21). Although proven to have significant clinical benefits, some studies demonstrated that Trastuzumab can cause myocardial damage, reducing the contractility of the left ventricle (22). Thus, various drug delivery systems have been developed in order to minimize its adverse effects especially with the use of polymeric nanoparticles and magnetic nanoparticles (4,31).

Magnetic nanoparticles arouse especial interest due to their high biocompatibility, super paramagnetic properties at room temperature, and versatile binding properties, allowing controlled attachment of bioactive molecules on NPs surface (38,39). In addition, iron oxide nanoparticles (Spion) are known to have little or insignificant toxic effect *in vitro* and *in vivo*, as well as suitable diffusion properties through tissues (15,42), and can be used as hyperthermic agents for local treatment of tumors (3,6,25). Despite such favorable chemistry, the simultaneous control of the surface chemistry and colloidal stability is not an easy task, and very few well characterized multi-functionalized nanosystems have been reported, particularly considering targeted nanoagents for application in diagnostic by image (28,33,41).

The use of radionuclides have been commonly described for both, diagnosing and treatment of tumors, been considered the perfect use of both features as a theragnostic agent. In fact, there is an increasing demand for new materials capable to enhance modern diagnostic techniques, delivering more precise and sensitive results, at similar or lower cost, and with a therapy approach, acting as a theragnostic (13,19,26).

Nevertheless, to achieve such goal it is fundamental to develop a platform for production of multi-functionalized diagnostic nanoagents able to recognize and bind selectively to structures, substructures and/or molecules expressed by specific tumor cells and tissues concentrating in them, thus simultaneously allowing the precise diagnosis (evaluation of the localization, size, morphology, as well as the cellular and molecular type) and treatment of tumors. For example, targeted nanoparticles were prepared and studied as imaging agents by Sarcinelli *et al.* (32) for breast cancer and Ligiero *et al.* (18) for GIST (Gastrointestinal stromal tumor) cancer.

In order to contribute with the advancement of this exciting and highly relevant field, here we described a fully dispersible iron oxide nanoparticle simultaneously decorated with Trastuzumab (TZMB) and diethylene triamine pentaacetic acid (DTPA), that we decided to call as: DTPA-TZMB@Fe_3O_4. The DTPA-TZMB@Fe_3O_4 can be conveniently labeled with Technetium-99m generating a SPECT nanoradiopharmaceutical (^{99m}Tc-DTPA-TZMB@Fe_3O_4 nanoparticles) suitable for early diagnosis and staging of breast cancer since combines the well-known low toxicity of SPIONs and no apparent adverse effects (14,38), with conventional radiolabeling protocols, good stability, fast renal clearance and high selectivity by breast cancer tumors. Also the DTPA-TZMB@Fe_3O_4 can be radiolabeled with Ga-68, forming the Ga-68-DTPA-TZMB@Fe_3O_4 nanoparticles a nanoradiopharmaceutical, that can also be used for PET imaging (5,10,27,29,34).

METHODOLOGY

Bis-Conjugated Magnetite Nanoparticles

Magnetite nanoparticles with average diameter of 8–10 nm ± 1.6 (Fig. 1) were prepared according to previously described method (12,36,38,39). These nanoparticles have primary amine reactive groups allowing conjugation with proteins, peptides, antibodies as well as other molecules possessing suitable functional groups. The strategy used to prepare the dual labeled targeted SPION is shown in Scheme 1. Fully dispersible amine-terminated SPIONs were prepared by attaching phosphorylethanolamine (PEA) to nanoparticles surface, and then reacted with DTPA in sub-stoichiometric amount (20:1 amine to DTPA). Then, the NPs were reacted with a large excess of GA – Glutaraldehyde – (10 fold) to convert the remaining amine groups in aldehyde derivatives that can be used to couple TZMB. This was reacted in stoichiometric amount with the iron oxide nanoparticles, yielding the bis-functionalized (DTPA and TZMB) and completely dispersible DTPA-TZMB@Fe_3O_4 nanoparticles (Fig. 2). It is

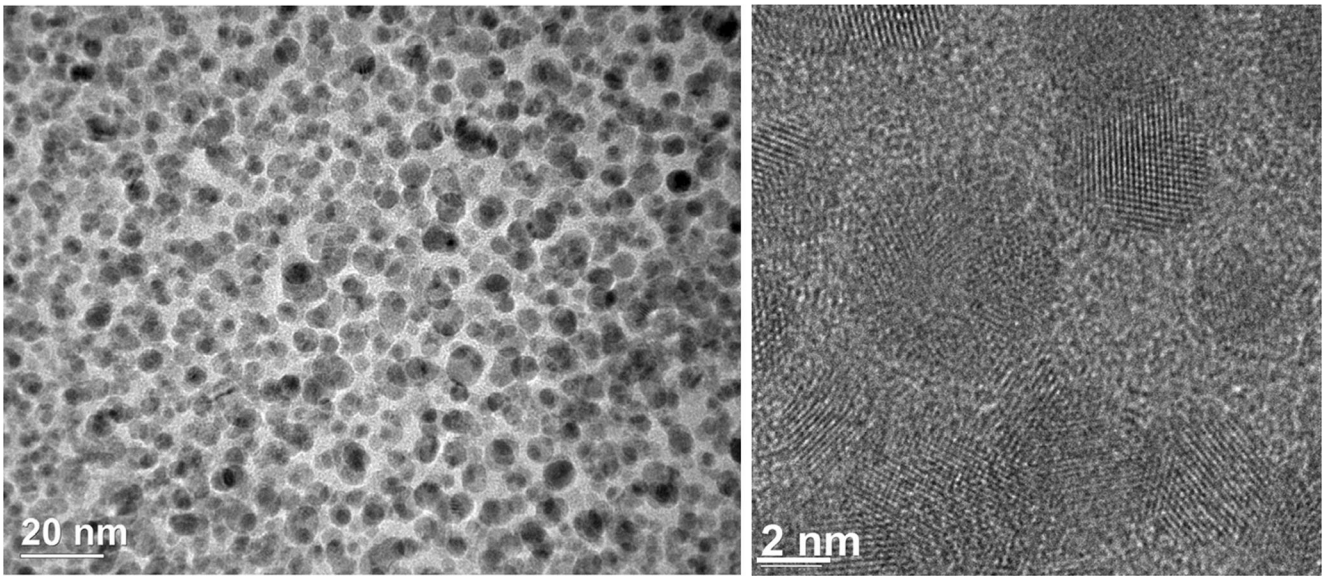

Fig. 1 TEM and HRTEM images of functionalized iron oxide nanoparticles, showing their quasi-spherical shape and high degree of crystallinity.

possible to observe that the decoration process allowed a great hydrodynamic behavior with no variation of size, as well as great dispersibility. It is also important to notice that even after the decoration process no formation of agglomerates was observed. Nevertheless the decoration process did not interfere in the size, shape and physical-chemical properties of the Spion. These were finally labeled with Tc-99m and Ga-68 to generate the targeted SPECT or PET labeled iron oxide nanoparticles.

LABELING PROCESS USING TECHNETIUM-99M AND GA-68

Labeling with 99mTc

The DTPA-TZMB@Fe_3O_4 nanoparticles were labeled by a direct method, as described by Rosa *et al.* (30) and Albernaz *et al.* (1), incubating 150 μL of DTPA-TZMB@Fe_3O_4 nanoparticles suspension 100 mCi

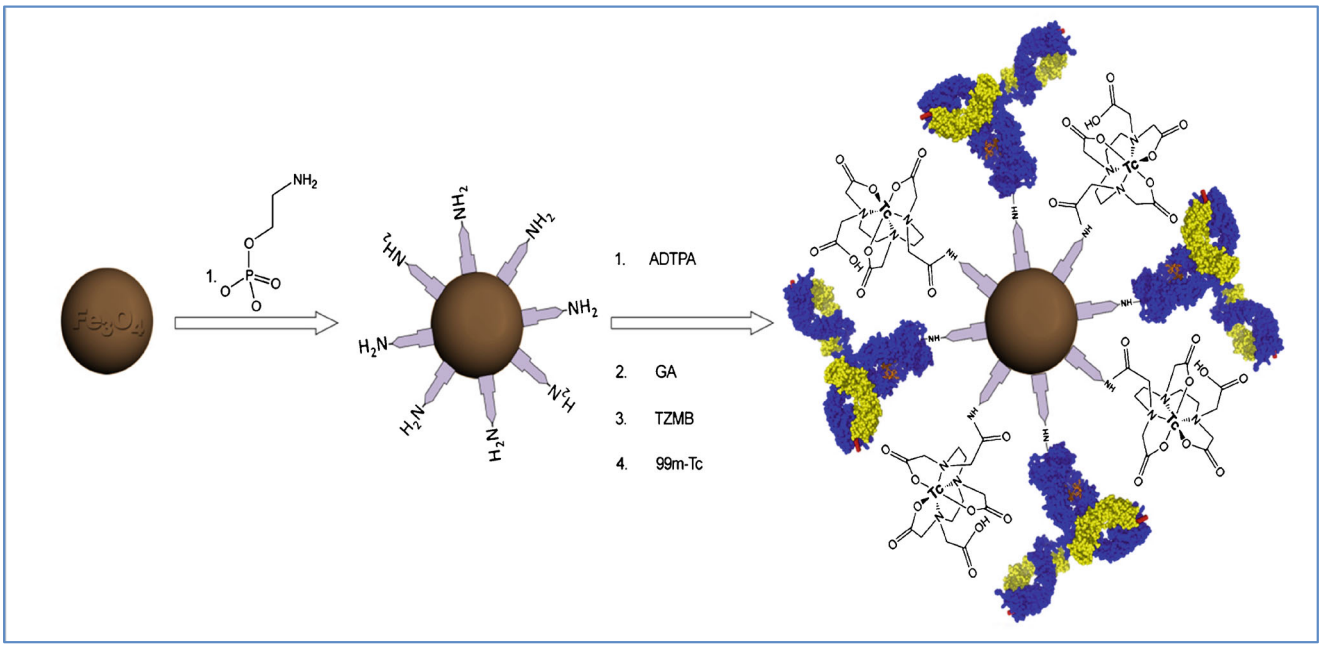

Scheme 1 Scheme showing the preparation of water dispersible iron oxide nanoparticles functionalized with DTPA and Trastuzumab, DTPA-TZMB@Fe_3O_4. Note that this is just a pictorial representation to show the components and how they were assembled.

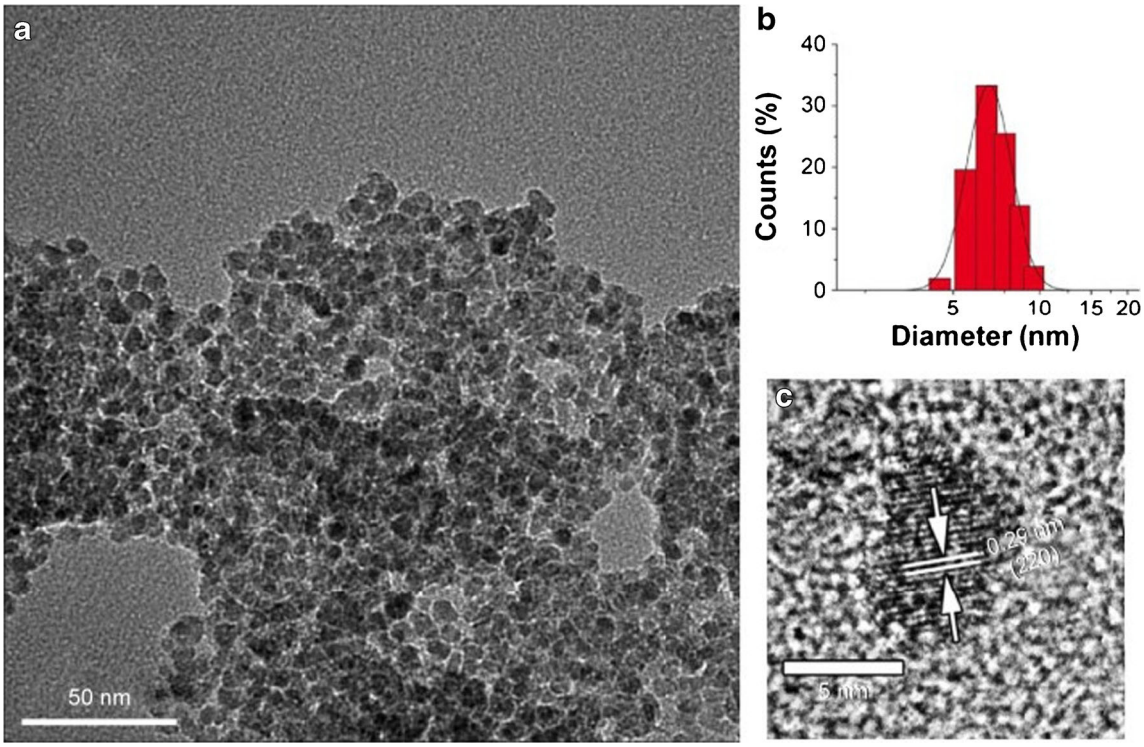

Fig. 2 (**a**) TEM images of functionalized iron oxide nanoparticles showing the size and shape; (**b**) Dynamic Light Scattering (DLS) result confirming the size and the hydrodynamic behavior; and C: High resolution transmission electron microscopy showing the surface of Spion as the distance between the nanoparticles, corroborating that no agglomerates has been formed. The arrows indicates the interplanar distance of 0.29 nm in the magnetite 220 crystal plane.

(approximately 300 μL) of technetium-99m (IPEN/CNEN) for 10 min. At the end of this procedure the iron oxide nanoparticles were labeled with Tc-99m generating ^{99m}Tc-DTPA-TZMB@Fe_3O_4 nanoparticles ready for use.

The labeled DTPA-TZMB@Fe_3O_4 nanoparticles were characterized by paper chromatography transferring 2 μl of ^{99m}Tc-DTPA-TZMB@Fe_3O_4 nanoparticles to Whatman paper n° 1 and eluting with acetone (Sigma-Aldrich) as mobile phase. The radioactivity distribution profile on the paper strips was verified in a gamma counter (Perkin Elmer Wizard® 2470, Shelton, CT City, State) in order to confirm the efficacy of the labeling process. The stability of the radiolabeling was verified incubating them for up to 8 h while monitoring by paper chromatography, as detailed above.

Labeling with Ga-68

The DTPA-TZMB@Fe_3O_4 nanoparticles were also labeled with Ga^{68}. In this case we used $Ga^{68}Cl_3$ as eluate obtained from an Eckert and Ziegler (IGG 100) Ge^{68}– Ga^{68} generator. The generator was fractionally eluted beginning with 5.0 ml of sterile 0.1 N HCl (Rotem). For fractional elution, the first 1.6 ml of eluate was discarded, the next 2.0 ml was collected for use and the final 1.4 ml was discarded. Two hundred fifty microlitre of the fractionated Ga-68 eluate (approximately 1.4 mCi / 52 MBq) was added to 100 μl of a 50% (*w*/*v*) solution of the DTPA-TZMB@Fe_3O_4 nanoparticles and allowed to incubate at room temperature (20 to 25°C) for 15 min. Following incubation, the DTPA-TZMB@Fe_3O_4 nanoparticles was tested for radiochemical purity.

Quality Control was performed using 12 cm strips of ITLC-SG (Varian) in 0.001 M HCl as the mobile phase. The Ga-68-DTPA-TZMB@Fe_3O_4 nanoparticles was spotted at one (1) cm and allowed to develop to the end of the strip. Nominal activity spotted on the strip was approximately 30 μCi (1.1 MBq). Once developed, the strip was cut in half and the two halves measured in a dose calibrator (Capintec CRC-25W). The Ga-68-DTPA-TZMB@Fe_3O_4 nanoparticle species remained at the origin and free Ga^6 Cl_3 migrating to the solvent front.

IN VIVO ANALYSIS

Tumor Xenografted Models

BT-474 cells (American Type Culture Collection, Manassas, VALLC) were cultured in RPMI (Gibco, Life technologies, MD, USA) supplemented with 10% of fetal bovine serum (Gibco, Life technologies, MD, USA) and 50 μg/mL of gentamicin (Gibco, Life technologies, MD, USA). Mycoplasma contamination in cultured cells was monitored using Lonza Mycoplasma Detection Kit. Was chosen BT-474 since it is a cell line that over-express HER-2 (35).

Tumors were implanted by subcutaneous (sc) injection of 2×10^6 cells at the right flank of 6-week-old female Balb/c nude mice. Tumor size was monitored for 3 weeks and measured with a caliper. The tumor size before imaging was about 2 cm large. Balb/c nude mice were bred at the animal facility of the Nuclear Energy Research Institute (IPEN) and all experiments complied with the relevant laws and were approved by local animal ethics committees. Mice were observed three times per week for evidence of distress, ascites, paralysis or excessive weight loss.

Biodistribution Studies

The biodistribution of ^{99m}Tc-DTPA-TZMB@Fe_3O_4 nanoparticles was evaluated considering two groups: a) the Control Group (healthy female Balb/c nude mice (n = 6) and Intervention Group (inducted female Balb/c nude (n = 6)). Mice were anesthetized with 15 μL of mix solution of 10% Ketamine and 2% Xylazine administered intramuscularly in the thigh. The ^{99m}Tc-DTPA-TZMB@Fe_3O_4 nanoparticles (3.7 MBq in 0.2 mL) was administered by retro-orbital via (18), and the mice of both groups were sacrificed by asphyxiation in a carbon dioxide gas chamber after 2 h (120 min). Organs (brain, lungs, kidneys, stomach, small and large intestine, bladder, heart and blood pool) were removed, weighted and the radioactivity in each organ and blood measured using a gamma counter (Perkin Elmer Wizard® 2470), and the results expressed as radiation activity per organ (%ID/organ).

Planar Imaging

Planar images were obtained 90 min post-retro-orbital injection of the ^{99m}Tc-DTPA-TZMB@Fe_3O_4 nanoparticles (3.7 MBq in 0.2 mL) in three mice (triplicate), integrating for 5 min the radiation counts centered at 140 KeV, with a Millennium Gamma Camera (GE Healthcare, Cleveland, USA), using a 15% window. The images were processed using *OsiriX* software, selecting specific regions of interest (ROIs) over the tumor for more detailed analysis.

RESULTS AND DISCUSSION

Labeling with 99mTc

The iron oxide nanoparticles functionalized with DTPA and TZMB (DTPA-TZMB@Fe_3O_4 nanoparticles), formed a stable colloidal suspension in aqueous solution and was successfully labeled (>90% yield) with 99mTc generating a clear suspension, with no evident precipitate, that passed readily through a 200 nm filter. The effectiveness of the labeling process was confirmed by paper chromatography which indicated almost no significant dissociation of technetium-99m from the ^{99m}Tc-DTPA-TZMB@Fe_3O_4 nanoparticles for a period as long as 8 h, as shown in Table I.

Labeling with Ga-68

The suitability of the DTPA-TZMB@Fe_3O_4 nanoparticles for labeling with Ga-68 was demonstrated by Instant Thin Layer Chromatography with Silica Gel (ITLC-SG) which indicated a radiochemical purity superior to 98%. This means that DTPA-TZMB@Fe_3O_4 nanoparticles may be applied as two-way imaging contrast agent by SPECT (Single Photon Emission Computer Tomography) and PET (Positron Emission Tomography). Unfortunately, it was not possible to make any PET imaging but the labeling results support their use as a PET nanoradiopharmaceutical.

Tumor Xenografted Model

A breast cancer tumor was successfully xenografted in the right flank of 6-week-old female Balb/c nude mice by subcutaneous (sc) injection of 2×10^6 BT-474 cells, and the volume of induced tumor monitored measuring with a caliper. The tumor was visible and palpable after 3 weeks.

Biodistribution Studies

Biodistribution studies are very important for defining the potential application of nanomaterials as delivery systems but also as contrast agents as discussed here. When administered by i.v. injection, or even by retro-orbital way, the nanoparticles will first interact with complex systems such as the body fluids and tissues, and eventually reach the desired target after overcoming the immune and clearance systems. In fact, the administered nanomaterial should circulate for long enough time for effective uptake and concentration by tumor tissues before been properly handled and cleared by the organism. This can be simulated by performing experiments using control mice without and with implanted tumor whereas the ability to overcome the defense and excretion systems and concentrate in the tumor, i.e. the targeting efficiency, can be evaluated in experiments with xenografted mice. Those experiments were carried out in triplicate using 6 mice (3 healthy

Table I Efficacy of the Labeling Process with 99mTc of DTPA-TZMB@Fe_3O_4 nanoparticles measured at every 2 h for up to 8 h

Time (h)	Labeling efficacy (%)
0	97,06
2	96,92
4	94,21
6	93,02
8	91,97

and 3 inducted) and the results expressed as percentage of dose per organ are depicted in Figs. 3 and 4.

The majority of radiolabeled ^{99m}Tc-DTPA-TZMB@Fe_3O_4 nanoparticles circulated in the blood and was uptake by the kidneys indicating that clearance by renal filtration is the most active excretion pathway. As expected, very small but still measurable amounts were also found in the blood and heart, as well as in the lung and spleen. However, it is interesting to mention that a significant amount was uptake by the small intestine while only minor amounts of radiation was detected in the liver, an organ that generally exhibits quite high affinity by and concentrate iron oxide nanoparticles, suggesting that the presence of TZMB antibody is protecting them from being recognized by Kupffer cells. Two hypothesis can be raised to explain the presence of nanoparticles in the small intestine: 1) there is a secondary intestinal excretion of ^{99m}Tc-DTPA-TZMB@Fe_3O_4 nanoparticles or its catabolites (24); or 2) there are HER2 receptors in the intestine (2,20,37) responsible for the recognition and concentration of that antibody.

The above described biodistribution is completely different from that obtained when cationic PEA@Fe_3O_4 nanoparticles were administered intravenous (IV) in healthy Wistar rats (38,39) leading to major and prolonged uptake by liver but with similar renal filtration uptake followed by rapid clearance from this organ. In fact, the presence of SPIONs was confirmed for about 4 months after injection of 50 mg/kg, or a month after injection of 10 mg/kg of body weight. This difference clearly indicates the key role of nanoparticles surface functionalization on the effectiveness of the nanoparticles for diagnostic purpose since the attachment of TZMB and DTPA to the same iron oxide core, instead of PEA, decreased dramatically the uptake by liver and directed almost all too fast excretion track through urine. This feature also suggests that ^{99m}Tc-DTPA-TZMB@Fe_3O_4 was almost invisible for the immune system probably allowing longer lifetime in the blood stream and a higher uptake by the tumor, as discussed below. Furthermore, no thrombus and immune response leading to unwanted interaction and incorporation of nanoparticles by endothelium and organs, except filtration by the kidneys, was observed in healthy mice.

The uptake by tumor of the decorated Spion, in the inducted breast cancer mice was 1.98 μCi (>20% of the total administered radioactivity), corroborating its use as a imaging agent It is possible to observe the renal clearance of the Spion in both cases (healthy and inducted mice) represented by the high uptake by the kidneys. It is also possible to observe, in both cases, the reduced uptake by the MPS (mononuclear phagocyte system) system represented by spleen and liver, corroborating the highly target Spion constructed. The larger amounts of 99mTc-TZMB@Fe_3O_4 nanoparticles in all organs when compared with the control group, corroborates that, although xenografted, the tumor induction altered the immune system of the mice. This may be notably visible by the uptake in the spleen. The markedly higher uptake by intestines (large and small) in the intervention group than in the control group corroborates the activation of the hepatobiliary excretion mechanism that was facilitated by the presence of TZMB, which, although is not free but immobilized on the iron oxide nanoparticles surface, activated the hepatobiliary via. Also is important to notice that breast cancer in early stages of metastasis may activate the over expression of HER-2 in other organs, like intestine and stomach and this must be considered in this case (8,11). In both cases there were uptake by the brain, and this may be explained by the fact that very small nanoparticles have a facilitated diffusion through the blood-brain barrier (23).

Planar Imaging

In the previous section the biodistribution based on sacrifice and biopsy of organs was described, indicating the concentration of 99mTc-DTPA-TZMB@Fe_3O_4 nanoparticles preferentially in the xenografted breast cancer tumor. Thus, a confirmation assay was carried out by planar imaging to corroborate the successful preparation of the

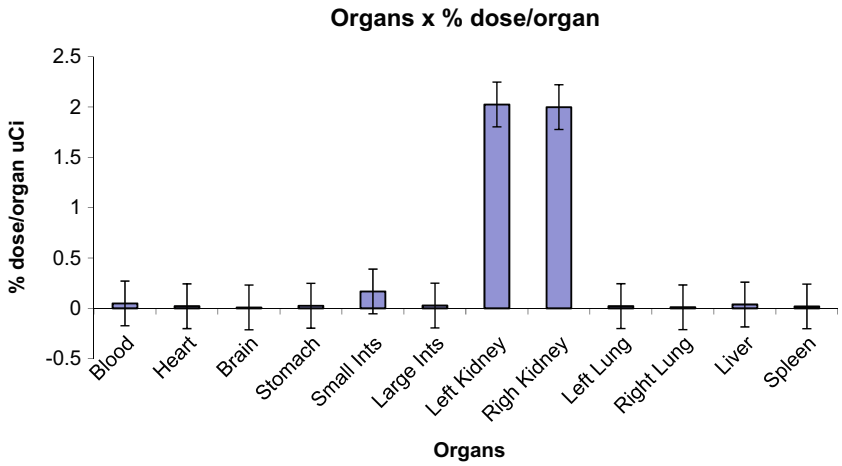

Fig. 3 Biodistribution of ^{99m}Tc-DTPA-TZMB@Fe_3O_4 nanoparticles in healthy female Balb/c nude mice (Control Group). The results are the average of three identical experiments.

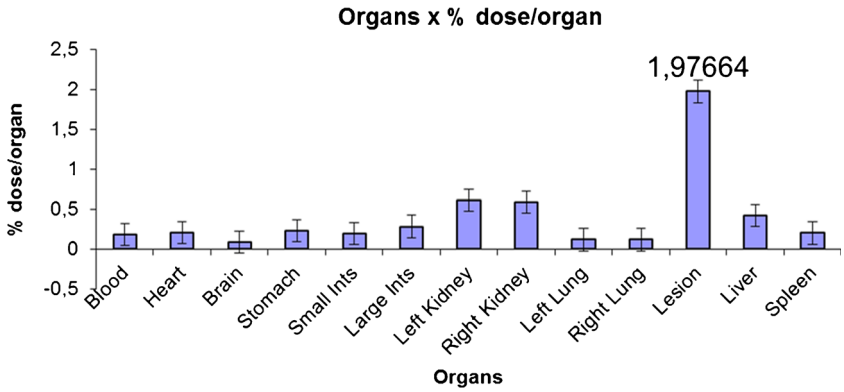

Fig. 4 Biodistribution of 99mTc-DTPA-TZMB@Fe_3O_4 nanoparticles in female Balb/c nude mice with xenografted breast cancer in the right flank (Intervention Group). The results are the average of three identical experiments.

^{99m}Tc-DTPA-TZMB@Fe_3O_4 nanoparticle. The images shown in Fig. 5 reveal three hyper capturing regions where the first one at the top (mice head) is the residual radioactivity in the injection site (retro-orbital administration). The most prominent one in the middle corresponds to the lesion. This result is consistent with the biodistribution data shown in Figs. 3 and 4 indicating that the major contribution is due to the concentration of ^{99m}Tc-DTPA-TZMB@Fe_3O_4 nanoparticles in the lesion but it is not possible to rule out the possibility of some contribution from the liver and spleen found is the same area. The third uptake region was assigned to the bladder and kidneys, as expected from the fact that more than 80% of the ^{99m}Tc-DTPA-TZMB@Fe_3O_4 nanoparticles is eliminated by renal clearance in the first 2 h, which was confirmed by the biodistribution data (Figs. 3 and 4) in the abdominal region.

In order to further confirm the uptake by the tumor, the lesion was excised 4 h after retro-orbital administration and imaged (Fig. 5), confirming the uptake by the tumor of ^{99m}Tc-DTPA-TZMB@Fe_3O_4 nanoparticles.

CONCLUSION

The high selectivity for the BT-474 cells induced xenografted tumor in female Balb/c nude mice, and in minor degree the almost no uptake by healthy mice, clearly indicated the successful preparation of 99mTc-DTPA-TZMB@Fe_3O_4 nanoparticles by successive conjugation of DTPA and TZMB on less than 10 nm diameter PEA@Fe_3O_4 nanoparticles, and the suitability of the labeling protocol with 99m-Tc and Ga-68, generating a promising multi-modal nano-radiopharmaceutical agent for

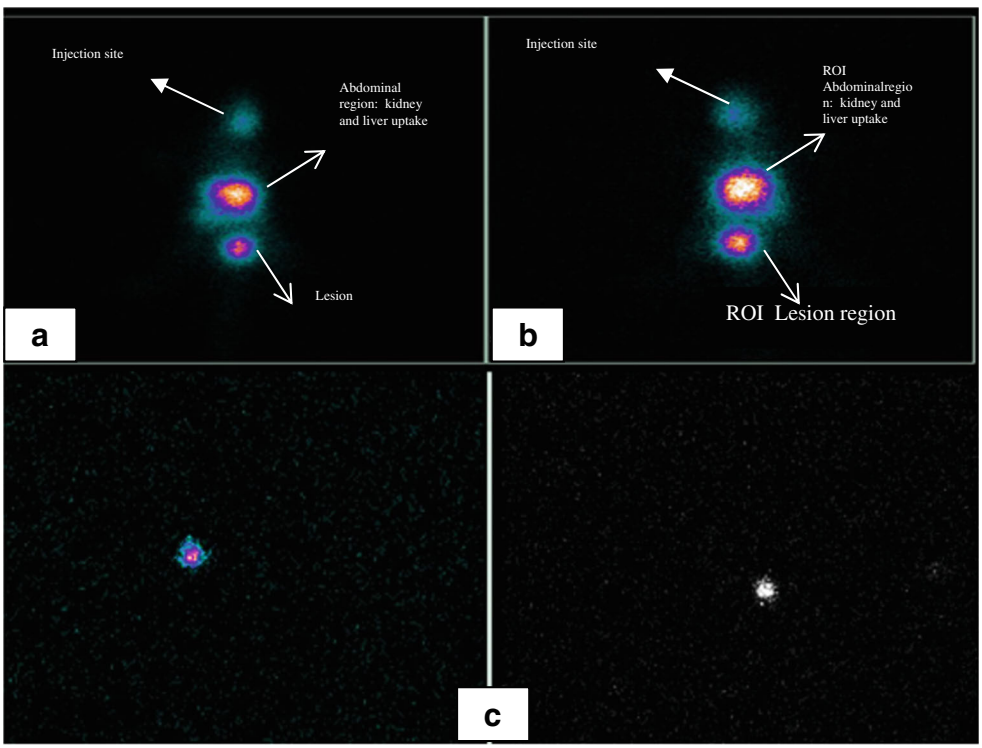

Fig. 5 Planar images of mice xenografted with breast tumor using the nano-radiopharmaceutical ^{99m}Tc-DTPA-TZMB@Fe_3O_4. In (**a**) we have the abdominal region showing the uptake by liver and spleen and the Lesion uptake. The calculated ROI region is shown also (**b**). It is possible to observe 3 uptake regions: the first in the top of the image regarded to the injection site (retro-orbital via). The second one in the middle regarding the abdominal image regarded to the liver, intestine, kidneys and spleen uptake. And the third one in the side of the animal regarding the tumor uptake. In (**c**) we have the planar image of excised lesion (breast tumor)from xenografted mice 4 h post retro-orbital administration of ^{99m}Tc-DTPA-TZMB@Fe_3O_4 nanoparticles.

in vivo diagnostic of breast cancer by PET and SPECT imaging, as well as by MRI as demonstrated in a previous publication. Those exciting features were obtained with a new engineered material based on biocompatible iron oxide nanoparticles exhibiting no apparent toxic effects, but more in depth studies on the imaging capability and toxicological effects should be carried out to confirm the safety and suitability for diagnostic purposes.

ACKNOWLEDGMENTS AND DISCLOSURES

Authors thankfully acknowledge Conselho Nacional de Desenvolvimento Científico e Tecnológico (CNPq) and Fundação de Amparo à Pesquisa do Estado de São Paulo (FAPESP) for the financial support.

REFERENCES

1. Albernaz MS, Ospina CA, Rossi AM, Santos-Oliveira R. Radiolabelled nanohydroxyapatite with 99m Tc: perspectives to nanoradiopharmaceuticals construction. Artif Cells Nanomed Biotechnol. 2014;42(2):88–91.
2. Alirezapour B, Jalilian AR, Rajabifar S, Mirzaii M, Moradkhani S, Pouladi M, *et al.* Preclinical evaluation of [11In]-DOTA-trastuzumab for clinical trials. J Cancer Res Ther. 2014;10(1):112–20.
3. Altanerova U, Babincova M, Babinec P, Benejova K, Jakubechova J, Altanerova V, *et al.* Human mesenchymal stem cell-derived iron oxide exosomes allow targeted ablation of tumor cells via magnetic hyperthermia. Int J Nanomedicine. 2017;12:7923–36.
4. Bordim A, Patricio BFC, Sarcinelli MA, Albernaz MS, Santos-Oliveira R. Nanoradiopharmaceuticals: development of labeling process for polymeric nanoparticles. Anal Oncol. 2013;2(1):30–3.
5. Bouziotis P, Stellas D, Thomas E, Truillet C, Tsoukalas C, Lux F, *et al.* ^{68}Ga-radiolabeled AGuIX nanoparticles as dual-modality imaging agents for PET/MRI-guided radiation therapy. Nanomedicine (London). 2017;12(13):1561–74.
6. Bretcanu O, Miola M, Bianchi CL, Marangi I, Carbone R, Corazzari I, *et al.* In vitro biocompatibility of a ferrimagnetic glass-ceramic for hyperthermia application. Mater Sci Eng C Mater Biol Appl. 2017;73:778–787. https://doi.org/10.1016/j.msec.2016.12.105.
7. Costa M, Saldanha P. Risk reduction strategies in breast cancer prevention. Eur J Breast Health. 2017;13(3):103–12.
8. English DP, Roque DM, Santin AD. HER2 expression beyond breast cancer: therapeutic implications for gynecologic malignancies. Mol Diagn Ther. 2013;17(2):85–99.
9. Eqqvist J. Nanoparticles as theranostic vehicles in experimental and clinical applications—focus on prostate and breast cancer. Int J Mol Sci. 2017;18(5):1102.
10. Evertsson M, Kjellman P, Cinthio M, Andersson R, Tran TA, In't Zandt R, *et al.* Combined Magnetomotive ultrasound, PET/CT, and MR imaging of ^{68}Ga-labelled superparamagnetic iron oxide nanoparticles in rat sentinel lymph nodes in vivo. Sci Rep. 2017;7(1):4824.
11. Freudenberg JA, Wang Q, Katsumata M, Drebin J, Nagamoto I, Greene MI. The role of HER2 in early breast cancer metastasis and the origins of resistance to HER2-targeted therapies. Exp Mol Pathol. 2009;87(1):1–11.
12. Gao H, Liu X, Tang W, Niu D, Zhou B, Zhang H, *et al.* ^{99m}Tc-conjugated manganese-based mesoporous silica nanoparticles for SPECT, pH-responsive MRI and anti-cancer drug delivery. Nano. 2016;8(47):19573–80.
13. Ghasemi M, Nabipour I, Omrani A, Alipour Z, Assadi M. Precision medicine and molecular imaging: new targeted approaches toward cancer therapeutic and diagnosis. Am J Nucl Med Mol Imaging. 2016;6(6):310–27.
14. Hamoudeh M, Kamleh MA, Diab R, Fessi H. Radionuclides delivery systems for nuclear imaging and radiotherapy of cancer. Adv Drug Deliv Rev. 2008;60(12):1329–46.
15. Jarockyte G, Daugelaite E, Stasys M, Statkute U, Poderys V, Tseng T-C, *et al.* Accumulation and toxicity of superparamagnetic iron oxide nanoparticles in cells and experimental animals. Int J Mol Sci. 2016;17(8):1193.
16. Lam DL, Houssami N, Lee JM. Imaging surveillance after primary breast cancer treatment. AJR Am J Roentgenol. 2017;208(3):676–86.
17. Ligiéro TB, Albernaz MS, Carvalho SM, Oliveira SMV, Santos-Oliveira R. Monoclonal antibodies: application in radiopharmacy. Curr Radiopharm. 2013;6:231–48.
18. Ligiero TB, Cerqueira-Coutinho C, Albernaz MS, Szwed M, Bernardes ES, Wasserman MAV, *et al.* Diagnosing gastrointestinal stromal tumours by single photon emission computed tomography using nanoradiopharmaceuticals based on bevacizumab monoclonal antibody. Biomed Phys Eng Express. 2016;2(4):045017.
19. Loi S, de Azambuja E, Pugliano L, Sotitiou C, Piccart MJ. HER2-overexpressing breast cancer: time for the cure with less chemotherapy? Curr Opin Oncol. 2011a;23(6):547–58.
20. Lub-de Hooge MN, Kosterink JG, Perik PJ, Nijnuis H, Tran L, Bart J, *et al.* Preclinical characterisation of 111IN-DTPA-trastuzumab. Br J Radiol. 2004;143:99–106.
21. Nahta R, Esteva FJ. HER-2-targeted therapy: lessons learned and future directions. Clin Cancer Res. 2003;9:5078–84.
22. Nahta R, Esteva FJ. Herceptin: mechanisms of action and resistance. Cancer Lett. 2006;232(2):123–38.
23. Nasr SH, Kouyoumdjian H, Mallett C, Ramadan S, Zhu DC, Shapiro EM, *et al.* Detection of β-amyloid by sialic acid coated bovine serum albumin magnetic nanoparticles in a mouse model of Alzheimer's Disease. Small. 2017. https://doi.org/10.1002/smll.201701828.
24. Oude Munnick TH, Dijkers EC, Netters SJ, Lub-de Hooge MN, Brouwers AH, Haasjes JG, *et al.* Trastuzumab pharmacokinetics influenced by extent human epidermal growth factor receptor 2 – positive tumor load. J Clin Oncol. 2010;28(21):e355–6.
25. Paudel NR, Shvydka D, Parsai EI. A novel property of gold nanoparticles: free radical generation under microwave irradiation. Med Phys. 2016;43(4):1598.
26. Pelaz B, Alexiou C, Alvarez-Pueble RA, Alves F, Andrews AM, Ashraf S, *et al.* Diverse applications of nanomedicine. ACS Nano. 2017;11(3):2313–238.
27. Pellico J, Lechuga-Vieco AV, Almarza E, Hidalgo A, Mesa-Nuñez C, Fernández-Barahona I, *et al.* In vivo imaging of lung inflammation with neutrophil-specific $_{68}$Ga nano-radiotracer. Sci Rep. 2017;7(1):13242.
28. Poller JM, Zaloga J, Schreiber E, Unterweger H, Janko C, Radon P, *et al.* Selection of potential iron oxide nanoparticles for breast cancer treatment based on in vitro cytotoxicity and cellular uptake. Int J Nanomedicine. 2017;12:3207–20.
29. Rainone P, Riva B, Belloli S, Sudati F, Ripamonti M, Verderio P, *et al.* Development of $_{99m}$Tc-radiolabeled nanosilica for targeted detection of HER2-positive breast cancer. Int J Nanomedicine. 2017;12:3447–61.
30. Rosa TG, Dos Santos SN, De Jesus Andreoli Pinto T, DDM G, Barja-Fidalgo TC, Ricci-Junior E, *et al.*

Microradiopharmaceutical for metastatic melanoma. Pharm Res. 2017; https://doi.org/10.1007/s11095-017-2275-3.
31. Sá LTM, Simmons S, Missailidis S, Silva MIP, Santos-Oliveira R. Aptamer-based nanoparticles for câncer targeting. J Drug Target. 2013;21(5):427–34.
32. Sarcinelli MA, Albernaz MS, Szwed M, Iscaife A, Leite KR, Junqueira MS, *et al.* Nanoradiopharmaceuticals for breast cancer imaging: development, characterization, and imaging in inducted animals. OncoTargetsTher. 2016;23(9):5847–54.
33. Serkova NJ. Nanoparticle-based magnetic resonance imaging on tumor-associated macrophages and inflammation. Front Immunol. 2017;8:590.
34. Silva F, Gano L, Cabral Campello MP, Marques R, Prudêncio I, Zambre A, *et al.* In vitro/in vivo "peeling" of multilayered aminocarboxylate gold nanoparticles evidenced by a kinetically stable ^{99m}Tc-label. Dalton Trans. 2017;46(42):14572–83.
35. Subik K, Lee JF, Baxter L, Strzepek T, Costello D, Crowley P, *et al.* The Expression patterns of ER, PR, HER2, CK5/6, EGFR, Ki-67 and AR by immunohistochemical analysis in breast cancer cell lines. Breast Cancer (Auckl). 2010;4:35–41.
36. Toma SH, Santo JJ, Araki K, Toma HE. Pushing the SERS sensitivity using superparamagnetic iron oxide nanoparticles: a non core-shell approach. Anal Chim Acta. 2015;855:70–5.
37. Tran T, Engfeldt T, Orlova A, Sandström M, Feldwisch J, Abrahmsén L, *et al.* (99m)Tc-maEEE-Z(HER2:342), an Affibody molecule-based tracer for the detection of HER2 expression in malignanttumors. Bioconjug Chem. 2007;18(6):1956–64.
38. Uchiyama MK, Toma SH, Rodrigues SF, Shimada AL, Loiola RA, Cervantes-Rodríguez HJ, *et al.* Ultrasmall cationic superparamagnetic iron oxide nanoparticles as nontoxic and efficient MRI contrast agent and magnetic-targeting tool. Int J Nanomedicine. 2015;10:4731–46.
39. Uchiyama MK, Toma SH, Cardoso RM, Rodrigues SF, Shimada ALB, Loiola RA, *et al.* Nanoparticles and their use as MRI contrast agent, BR102015013031–7, 08/06/2015.
40. Urban LABD, Chala LF, Bauab SDP, Schaefer MB, Dos Santos RP, Maranhão NMA, *et al.* Breast cancer screening: updated recommendations of the Brazilian College of Radiology and Diagnostic Imaging, Brazilian Breast Disease Society, and Brazilian Federation of Gynecological and Obstetrical Associations. Radiol Bras. 2017;50(4):244–9.
41. Yang R-M, C-P FU, Fang J-Z, Xu X-D, Wei X-H, Tang W-J, *et al.* Hyaluronan-modified superparamagnetic iron oxide nanoparticles for bimodal breast cancer imaging and photothermal therapy. Int J Nanomedicine. 2017;12:197–206.
42. Zhang Y, Kohler N, Zhang M. Surface modification of superparamagnetic magnetite nanoparticles and their intracellular uptake. Biomaterials. 2002;23:1553–61.